Proceedings of the SEM Annual Conference
June 1-4, 2009 Albuquerque New Mexico USA

Mixed-Mode Crack Growth in Ductile Thin Sheet Materials

J.H Yan[1], M. A. Sutton, X. Deng, Pablo Zavattieri* and Z.G Wei

Department of Mechanical Engineering, University of South Carolina, Columbia, SC 29208
[1] yan@cec.sc.edu (J.H. Yan)
*GM Research and Development Center, Warren, MI 48090

Abstract
The deformation of thin sheet aluminum and steel specimens subjected to mixed-mode I/III stable tearing experiments has been measured by using three-dimensional digital image correlation (3D-DIC). Features of crack growth in these mixed-mode I/III experiments are characterized, including (a) the specimen's deformed shape and 3D full-field surface displacement fields, (b) the load-crack extension curves and crack paths, (c) angular and radial distributions of polar strain components, and (d) COD variation as a function of crack extension. Results indicate that for the highly ductile aluminum and steel materials under remote mixed-mode I/III loadings (Φ=30°, 60°) or remote Mode III loading (Φ=90°) the deformations have almost identical angular and radial polar strain distributions, which are modified from those measured under nominal Mode I loading (Φ=0°). Results confirm that introduction of a Mode III loading component lowers the value of the dominant strain component ahead of the growing crack tip while increasing the radial singularity of the strain as compared with mode I loading. The mixed mode I/III average stable COD for AL6061-T6 (GM6208 steel) is 4X (3X) greater than measured during Mode I stable tearing in the same material, with clear correlations between the variation of COD with loading angle and that of the crack tip strain component during crack growth.

1. Introduction

Ductile thin sheet structural elements are oftentimes subjected to complex loading conditions in practical service situations that may involve a combination of tension, in-plane shear and torsion. A crack in such a component is therefore likely to be subjected to mixed mode loading conditions, resulting in stable crack growth (SCG) in the ductile material before instability sets in. Understanding such fracture events in ductile materials is an important component of structural integrity analysis for ductile thin-sheet structures. In recent years, mixed-mode I/III fracture has been the focus of many recent investigations [1-8] with most of the work on fracture toughness measurements and evaluation [7]. Due to the complex nature of mixed mode I/III fracture in ductile thin sheet materials [1-4, 8], there are limited experimental investigations and numerical simulations in the literature. Currently, there are no general fracture criteria available for mixed mode fracture of thin sheet ductile materials. A critical mixed mode I/II COD (crack tip opening displacement) has been shown to be a viable crack growth criterion for many ductile materials, including 2024-T3 aluminum alloy, under combined tension (mode I) and in-plane shear (mode II) loading conditions [9-10]. Limited literature exists regarding crack tip fields during stable crack growth for mixed mode I/III loading of thin-sheet ductile materials, even though such fields are expected to play a significant role in the fracture processes in thin structure under mixed-mode I/III loading conditions. The current study focuses on experimental measurements during tension-torsion loading of flawed ductile thin sheet aluminum and steel specimens to improve our understanding of the crack tip strain fields during stable tearing.

Specifically, three-dimensional digital image correlation (3D-DIC) [1,3,4] is employed to characterize the crack tip deformation fields during stable crack extension behavior in thin-sheet ductile specimens undergoing stable crack extension . Key results from these experiments are presented, including (a) 3D full-field surface displacement and strain fields, (b) crack path data in the un-deformed configuration of the specimens, and (c) critical generalized CTOD measurements as a function of crack extension.

2. Experimental procedures

Figure 1 shows the in-plane geometry of the pre-cracked, 2mm thick specimen used in the mixed-mode I/III experiments. All mixed mode I/III experiments were performed in an MTS 810 load frame under displacement control. Figure 2 presents a close-up of the 3D-DIC system and loading fixture used for displacement measurement in these experiments. Before performing each experiment, a high contrast random pattern is applied to each specimen, the 3D-DIC system is positioned to view the crack tip region and both cameras are synchronized and calibrated.

Prior to loading, a pair of un-deformed images of the top surface of the specimen is acquired as a reference for stereo-vision analysis using commercial software [11]. A coordinate system (X, Y, Z) with its origin at the pre-crack tip was defined on the un-deformed reference (see Fig 1), with (U, V, W) denoting the displacements along X, Y and Z, respectively. The 3D surface displacement fields were converted to in-plane strain fields (ε_{xx}, ε_{yy} and ε_{xy}) in the area of interest using the Lagrangian strain field formulation in terms of the displacement gradients [1]. In order to characterize the deformation and strain during crack growth, two coordinate systems are used in this study. Figure 3 presents the definition of polar coordinates, M(r, θ), relative to the (X, Y, Z) system at the current crack tip C_c and its relationship with the global (local) Cartesian coordinate system XOY defined in Fig.1. Here, O is located at the fatigue pre-crack tip, OX is along the pre-crack direction, and C_p is the previous crack tip position. Strain components (ε_{xx}, ε_{yy} and ε_{xy}) in the original configuration for point M (in Fig.3) are transformed to the components ($\varepsilon_{\theta\theta}$, ε_{rr} and $\varepsilon_{\theta r}$) in the polar coordinate system assuming that a planar state exists in the X-Y plane.

2. Results and discussion

The deformed shape of an AL6061-T6 specimen with about 20mm crack extension during a mixed mode I/III experiment at loading angle Φ=60° is shown in Figure 4. Figure 5 presents the crack path projected on the X-Y plane (the un-deformed specimen surface plane) for 2mm thick AL6061-T6 and GM6208 steel pre-cracked specimens undergoing quasi-static mixed mode I/III loading. It is seen that most of the crack paths are nearly straight and almost along the specimen center line; only the AL6061-T6 specimen loaded at Φ=90° is curved toward the upper (fixed) portion of the specimen. Load-actuator displacement curves during mixed mode I/III experiments are plotted in Fig.6. As shown in Fig. 6, the maximum tensile load during crack extension decreases with loading angle for both materials.

Figure 7 shows the various deformed shapes of the AL6061-T6 and GM6208 steel specimens during crack extension Δa for loading angles Φ=0°, 30°, 60° and 90° As shown in Fig. 7, even for mode I loading there exists significant out of plane specimen warping. Figure 8 shows contours of (U, V W) during crack extension in the AL6061-T6 specimens under quasi-static loading at Φ=0°, 30°, 60° and 90°. All displacement components are present in the displacement fields, with the out-of-plane displacement W and the in-plane crack-opening displacement V being relatively large. The dominant W-displacement component increases with increasing crack extension, with significant specimen rotation evident during crack extension.

To present radial and angular field variations around the current crack tip, a polar coordinate system is defined at each current crack tip as shown in Fig.4. Figures 9 and 10 show the representative angular and radial variations of strains ($\varepsilon_{\theta\theta}$, ε_{rr} and $\varepsilon_{\theta r}$) during crack extension in both AL6061-T6 and GM6208 specimens. Results for a growing crack indicate that all mixed-mode I/III loading cases (Φ =30°, 60^o and 90^o) have almost identical angular distributions, with (a) a single positive and negative maximum in each strain component, (b) maxima in the components occurring at different θ values and (c) the magnitudes of strain maxima are in the order $\varepsilon_{\theta\theta} > \varepsilon_{rr} > \varepsilon_{\theta r}$. It is also be seen that the measured strain fields during tension-torsion loading are clearly different from those measured during nominal Mode I loading.

The radial variation of $\varepsilon_{\theta\theta}$ in Figs.9 and 10 shows that $\varepsilon_{\theta\theta}$ increases sharply as $r \rightarrow 0$, suggesting a strain singularity near the crack tip. Figure 11 presents the near-tip variations of $\ln(\varepsilon_{\theta\theta})$ with $\ln(r)$ for various Δa values, where r is radial distance from the current crack tip. As shown in Fig.11, the data in a portion of the crack tip region is reasonably represented by a linear fit. The slopes obtained by least square fitting to the data are also presented in Fig.11. Fig.11 indicates that the hoop strain component $\varepsilon_{\theta\theta}$ for both pure tension and mixed mode I/III loading in both materials has a power-law type strain singularity near the crack tip. For the aluminum and steel specimens, the well-defined linear trends clearly show that the measured surface singularity under tension-torsion loading is higher than measured for tensile loading, demonstrating that at least one effect of combined mode I/III loading is to localize the large strains around the crack tip, an observation that suggests the need for further investigations.

The crack-tip opening displacement (COD) has been shown to be an effective fracture parameter in mixed mode I/II fracture of ductile thin-sheet materials [6]. In order to further understand the mixed mode I/III fracture of ductile thin-sheet materials, critical COD values were obtained by analyzing the images taken by the 3D-DIC system. Following procedures outlined in previous studies [1, 3], the local COD and its components on the surface of the specimen were calculated at 1mm behind the current crack-tip based on the crack-tip local coordinate system in the current deformed configuration. Figure12 presents a compilation of all measured total COD ($COD = \sqrt{COD_I^2 + COD_{II}^2 + COD_{III}^2}$) as a function of crack extension Δa for AL6061-T6 and GM6208 steel specimens under mixed mode I/III loading at Φ=0°, 30°, 60° and 90°. For both AL6061T6 and GM6208 specimens, COD data from different mixed mode I/III loading angle Φ=30°, 60° and 90° fall in a well-defined band, that is clearly separated from Mode I COD data. For Al6061T6, the mixed mode I/III average stable COD≈ 0.40mm and is 4× greater than the Mode I stable COD≈ 0.10mm. For steel specimen, the mixed mode I/III average stable COD≈ 0.65mm and is about 3× higher than the Mode I average stable COD≈ 0.23mm. These results indicate that the magnitude of the critical COD is a function of loading mode in highly ductile, thin sheet materials. Though the precise reason for the large increase in COD is not fully understood, it is believed that the large structural, out-of-plane bending introduced by the mode III component in combined tension-torsion loading contribute to the measured values of COD in these materials..

In light of the measured COD variation under mode I and mixed mode I/III loading, the radial variation of $\varepsilon_{\theta\theta}$ during mode I and mixed mode I/III loading in Figs. 9 and 10 demonstrates there is a direct correlation between variations in stable COD and the crack tip strain component $\varepsilon_{\theta\theta}$ during both crack initiation and stable crack growth for different loading modes. The larger and less singular crack tip strain component $\varepsilon_{\theta\theta}$ during mode I loading correlates with a smaller stable COD, while the lower and more singular crack tip component $\varepsilon_{\theta\theta}$ under mixed mode I/III loading corresponds to a large local COD. Taken together, changes in the deformation fields around the crack front introduced by the addition of a mode III component appear to be the basis for the increased critical CTOD value. The effect of large out-of-plane structural bending on fracture prediction will require additional studies in order to gain a full understanding.

3. Concluding remarks

With regard to the utility of the COD measurement for stable tearing predictions, it is noted that Wei [2] recently simulated mixed mode I/III fracture in thin sheet aluminum alloys and steel. The average value of the above measured COD at 1mm behind the moving crack front on the surface was used to simulate crack extension and crack path under mixed mode I/III loading. Results show that the average value of measured COD at 1mm behind the moving crack front on the surface is able to predict crack extension in thin-sheet specimens under remote mixed-mode I/III loading conditions. Furthermore, the in-plane COD vector on the mid-plane of the specimen was used to determine the crack growth paths and the prediction was in good agreement with the measured crack paths. These results suggest that the crack path under local mixed-mode I/II/III conditions is controlled by the in-plane COD components.

Acknowledgements

The support of General Motors Research is gratefully acknowledged. The authors are grateful to Dr. Wei Zhao for his work on the mixed-mode I/III loading fixture/specimen system and to Mr. Mathew J. Hammond for his assistance in conducting the mixed-mode I/III experiments.

References

1. Yan J -H, Sutton M A, Deng. X, Cheng C –S. Mixed-mode fracture of ductile thin-sheet materials under combined in-plane and out-of-plane loading, Int. J fracture 144: 297-321, 2007
2. Wei Z. Study of fracture in ductile thin sheets under remote I/III loadings. Ph.D dissertation, University of South Carolina, Columbia South Carolina, June 2008
3. Sutton M A, Yan J -H, Deng X, Cheng C-S, Zavattieri P. Three-dimensional digital image correlation to quantify deformation and crack-opening displacement in ductile aluminum under mixed-mode I/III loading. Optical Engineering 2007, 46(5): 051003, 2007
4. Wei Z, Yan J, Deng X, Sutton M A. Study of Mixed-Mode I/III Fracture in Ductile Materials. 2005 annual conference in Society of Experimental Mechanics, Portland, USA, July 2005.
5. Pan J., Shih C. F. Elastic-plastic analysis of combined mode I, II and III crack-tip fields under small-scale yielding conditions. International Journal of Solids and Structures, Volume 29, Issue 22, Pages 2795-2814, 1992

6. Zucchini A., Hui C Y And Zehnder Alan T. Crack tip stress fields for thin, cracked plates in bending, shear and twisting: A comparison of plate theory and three-dimensional elasticity theory solutions. International Journal of Fracture, 104: 387–407, 2000.
7. Kamat S. V., Srinivas M. and Rao P. Rama. Mixed mode I/III fracture toughness of Armco iron. Acta mater. Vol. 46, No. 14, pp. 4985-4992, 1998
8. Sutton M A, Helm JD, Boone ML. Experimental study of crack growth in thin sheet material under tension-torsion loading. Int J Fract, 109: 285-301, 2001
9. Sutton M A, Ma F, Deng X. Development and application of a CTOD-based mixed mode fracture criteria. Int J Solids Struct, 37: 3591-618, 2000
10. Sutton M A, Boone M L, Ma F, Helm J D A combined modeling-experimental study of the crack opening displacement fracture criterion for characterization of stable crack growth under mode I/II loading in thin sheet materials. Eng Fract Mech 66: 171-185, 2000.
11. VIC3D, Correlated Solutions Incorporated, 120 Kaminer Way, Parkway Suite A, Columbia, SC 29210, www.correlatedsolutions.com.

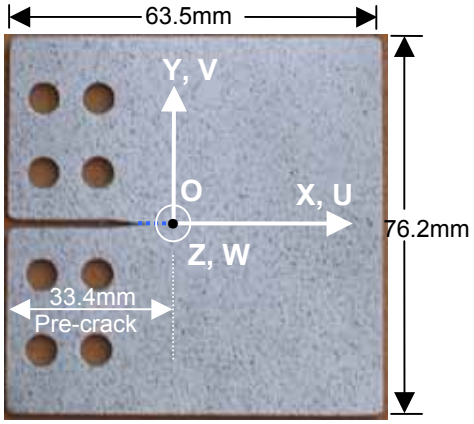

Fig.1: mixed I/III mode specimen and the global coordinate system. Origin O is at pre-crack tip.

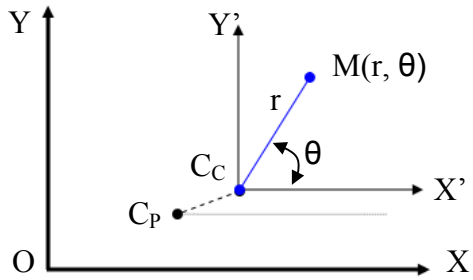

Fig.3: Definition of polar coordinate system M(r, θ) (under un-deformed configuration) at current crack tip Cc, where XOY (X'CcY') is the global (local) Cartesian coordinate system, O is at the fatigue pre-crack tip and OX is along the pre-crack direction, and Cp is the previous crack tip position

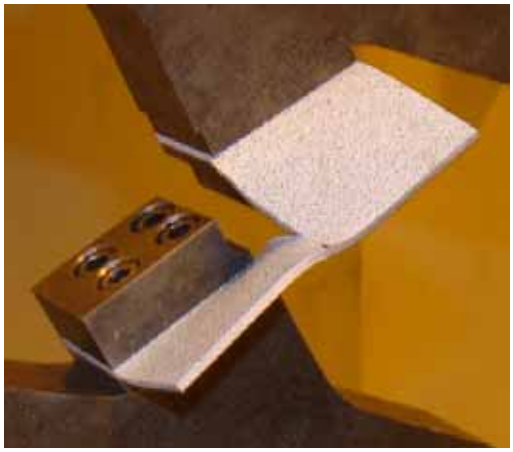

Fig.4: The deformed shape of an AL6061-T6 specimen with about 20mm crack extension during a mixed mode I/III experiment at loading angle Φ=60°.

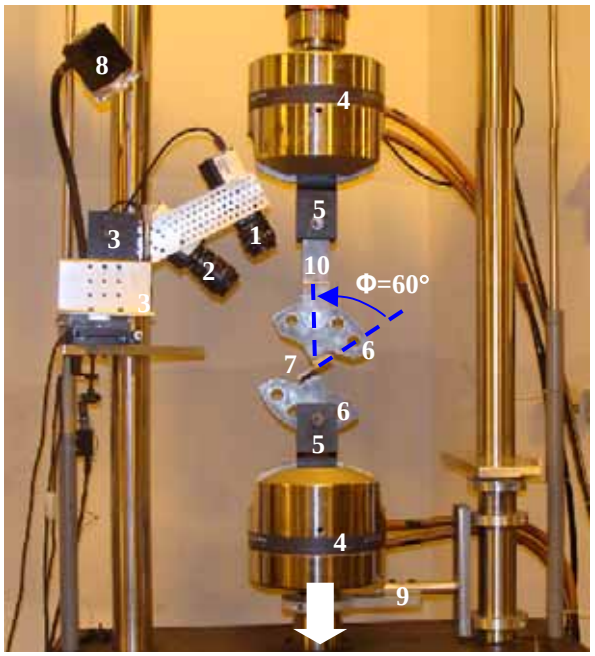

1—Camera 0, 2—Camera 1, 3—Translation Stage, 4—Hydraulic Grip 5—Clevis, 6—Fixture, 7—Specimen, 8—Light Source, 9-Rotation Constraint, 10—extension bar

Fig.2: The setup of quasi-static mixed I/III mode experiments with 3D displacement measurement system.

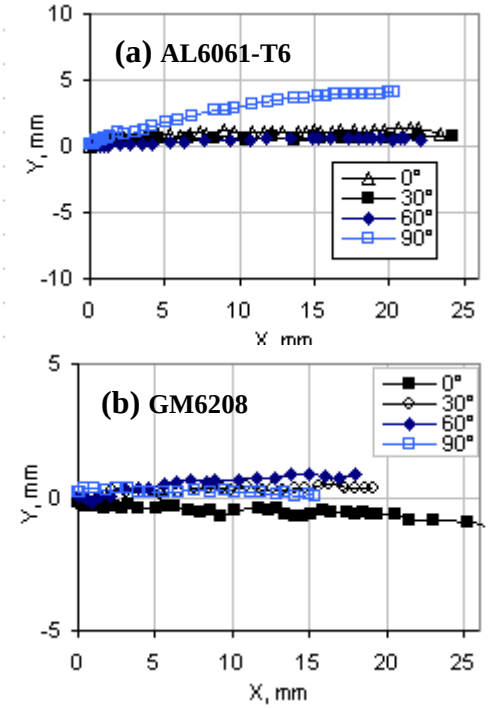

Fig.5: Crack paths in the un-deformed configuration for specimens loaded in mixed mode I/III.

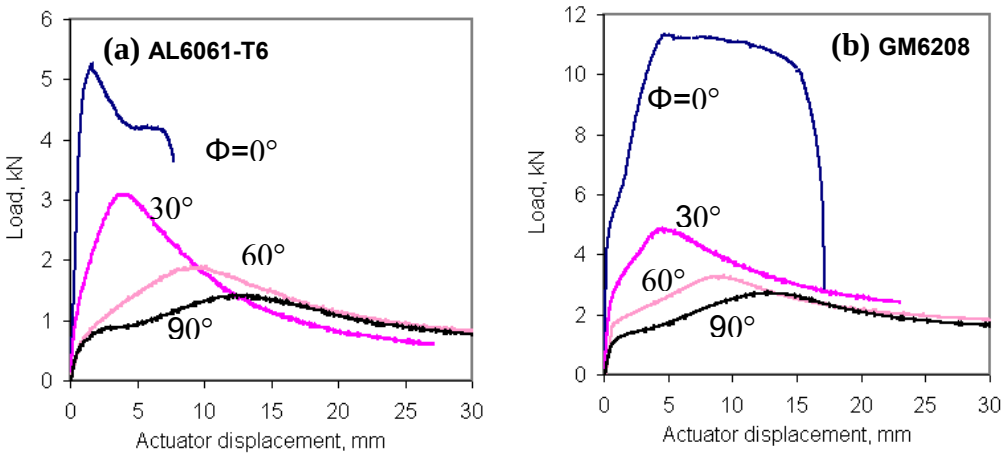

Fig.6: Load-MTS actuator displacement curves in mixed mode I/III experiments.

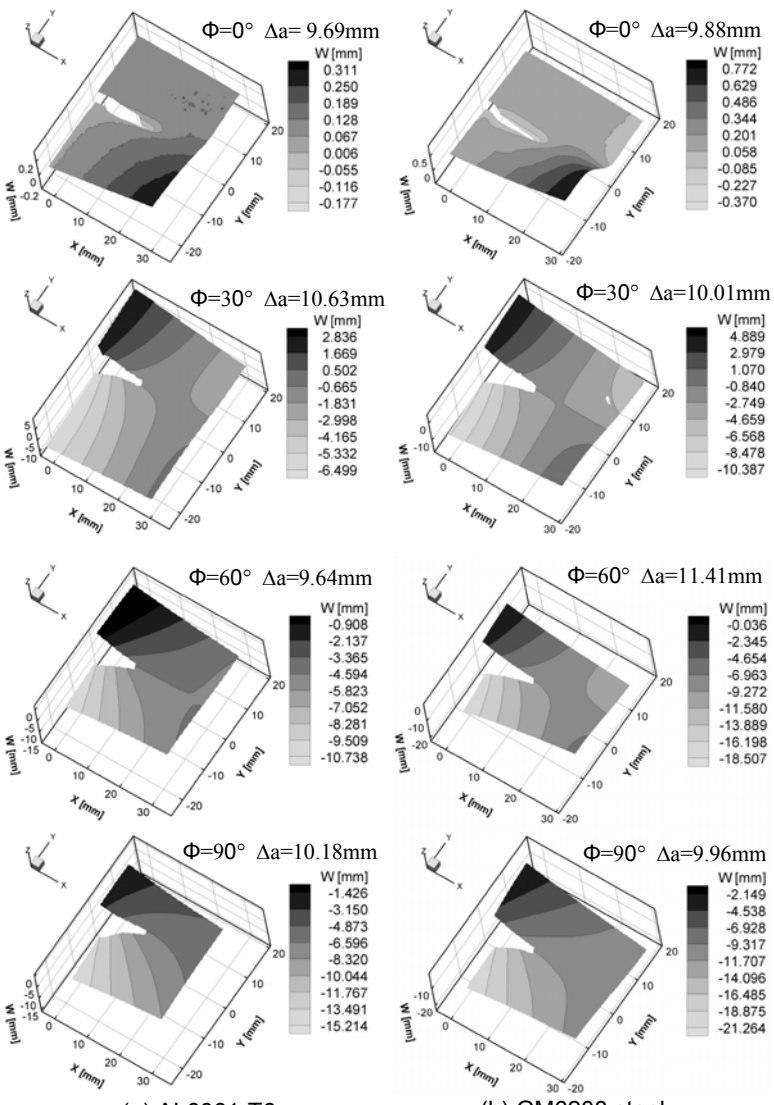

(a) AL6061-T6 (b) GM6208 steel

Fig.7: Deformed shapes for growing cracks with crack extension Δa during quasi-static mixed mode I/III experiments at Φ=0°, 30°, 60° and 90° for (a) AL6061-T6 and (b) GM6208 steel.

(a) Φ=0° Δa= 9.69mm

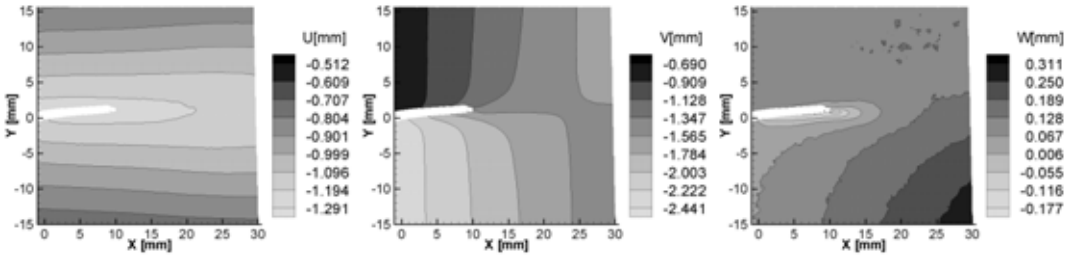

(b) Φ=30° Δa=10.63mm

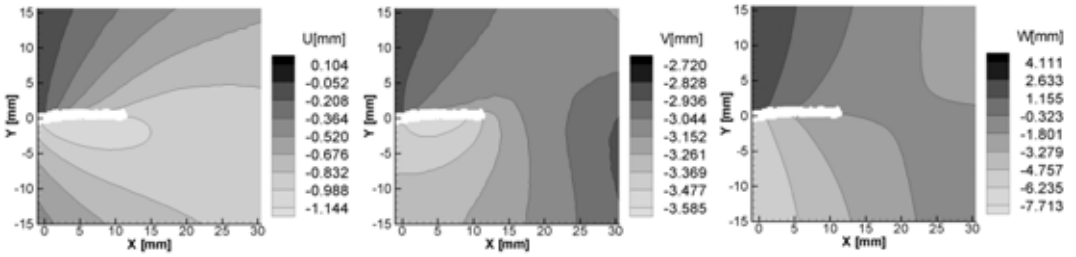

(c) Φ=60° Δa=9.64mm

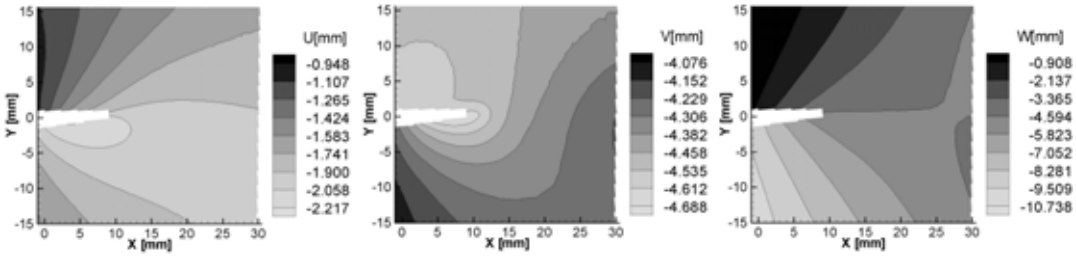

(d) Φ=90° Δa=10.18mm

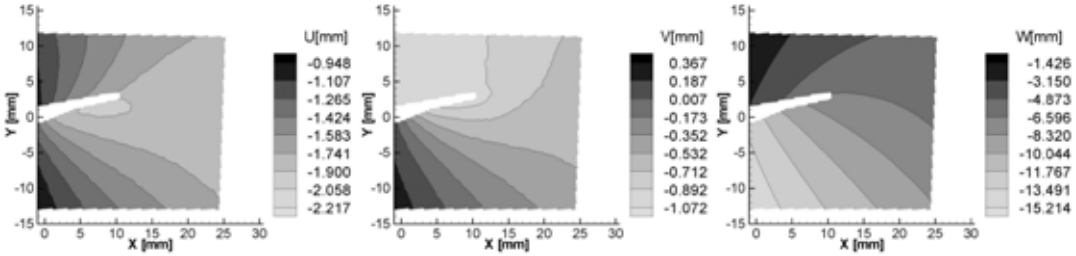

Fig.8: Contours of displacements for a growing crack extension Δa in 2-mm thick AL6061-T6 specimens under quasi-static loading at Φ=0°, 30°, 60° and 90° during mixed mode I/III experiments

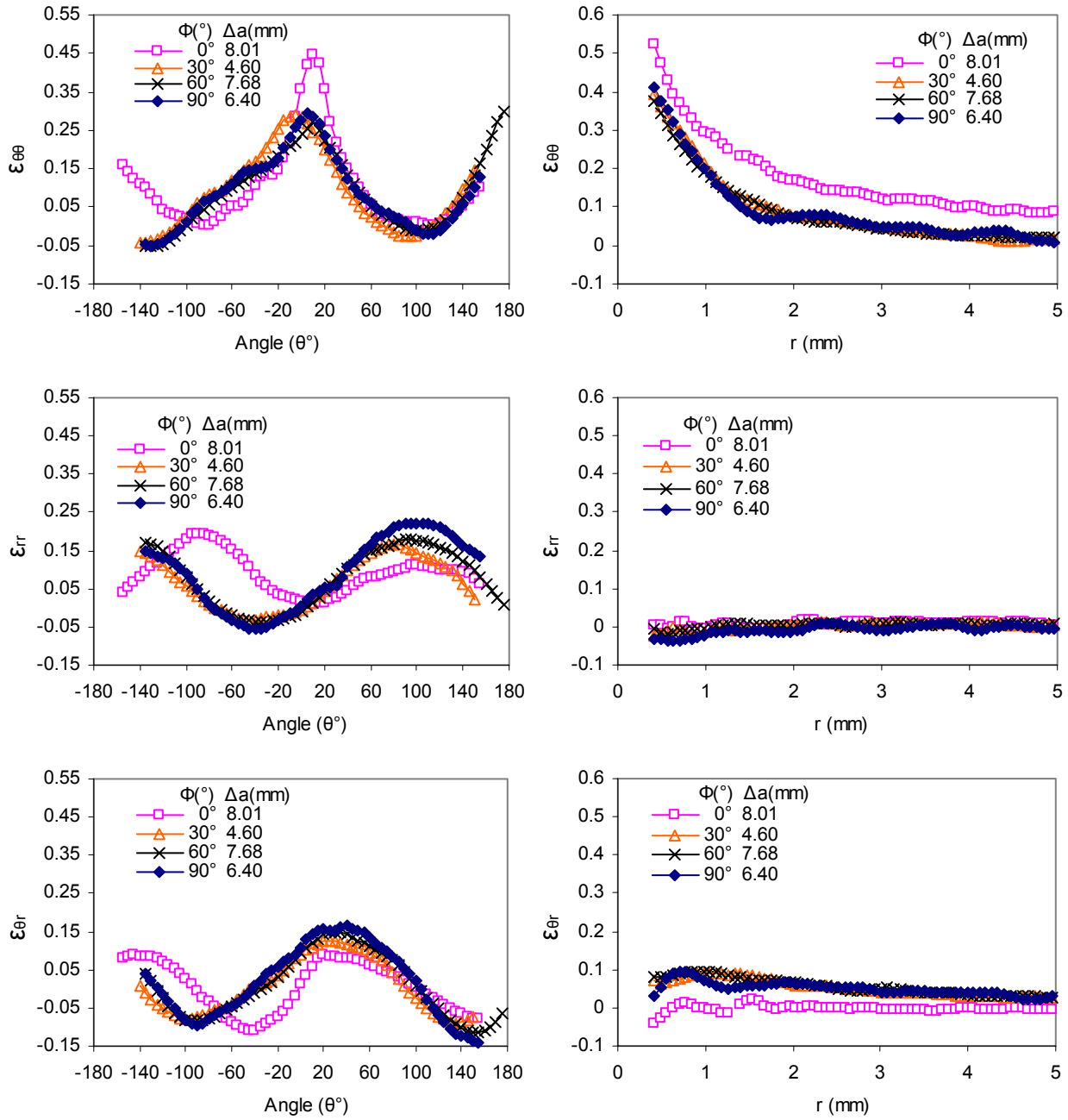

(a) Angular variations at r=0.75mm from current crack tip

(b) Radial variation

Fig.9: Angular and radial variations of surface strains as a function of crack extension in Φ=0°, 30°, 60° and 90° mode I/III experiment of a AL6061-T6 specimen, where r is the radial distance from the current crack tip (in the un-deformed configuration), and the angle θ=0° is along the global X-direction. (a) Angular variations at r=0.75mm from current crack tip. (b) Radial variation along θ=0°, -5°, 0° and -10° for Φ=0°, 30°, 60° and 90° respectively.

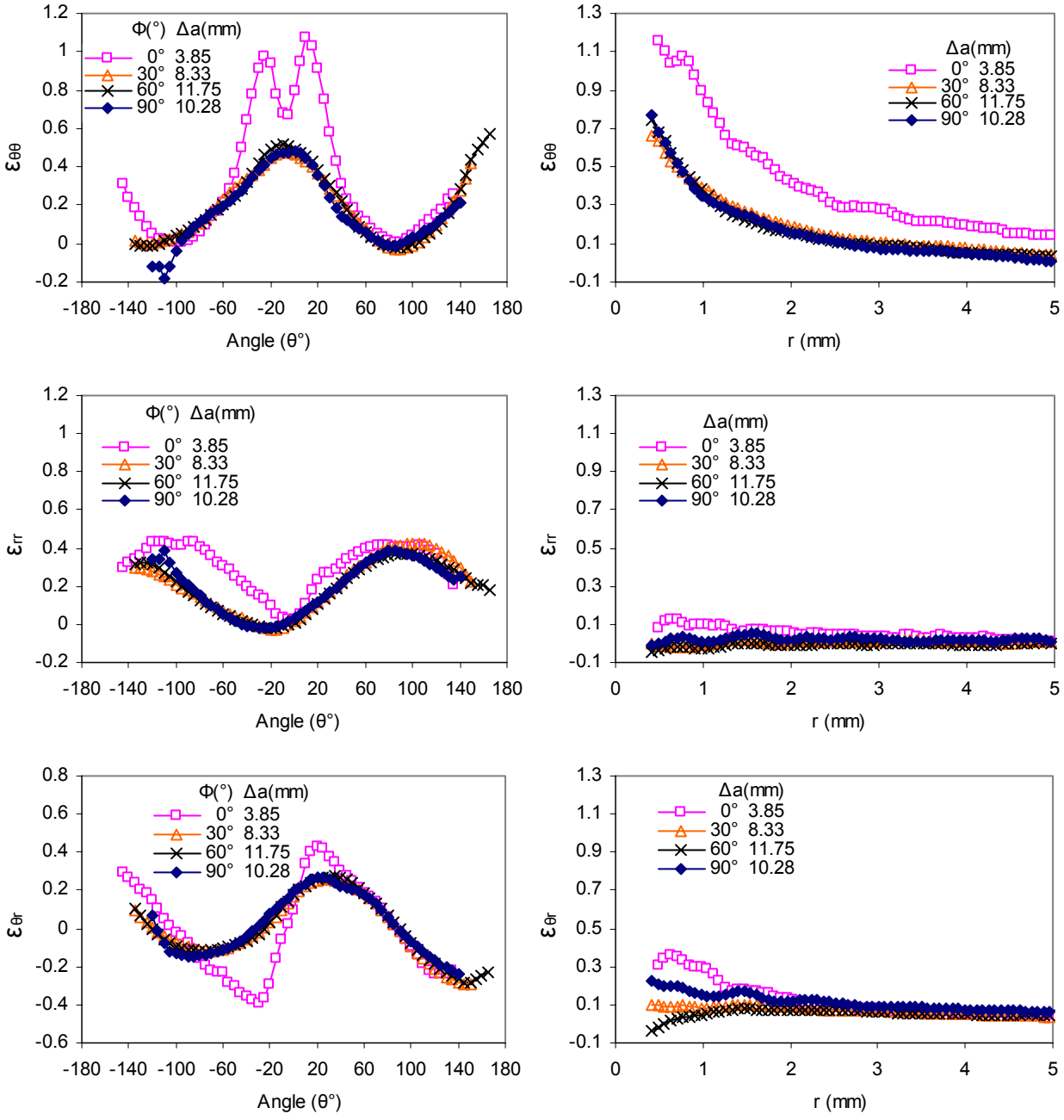

(a) Angular variations at r=0.75mm from current crack tip

(b) Radial variation

Fig.10: Angular and radial variations of surface strains as a function of crack extension in Φ=0°, 30°, 60° and 90° mode I/III experiment of a GM6208 steel specimen, where r is the radial distance from the current crack tip (in the un-deformed configuration), and the angle θ=0° is along the global X-direction. (a) Angular variations at r=0.75mm from current crack tip. (b) Radial variation along θ=0°, -10°, -20° and 0° for Φ=0°, 30°, 60° and 90° respectively.

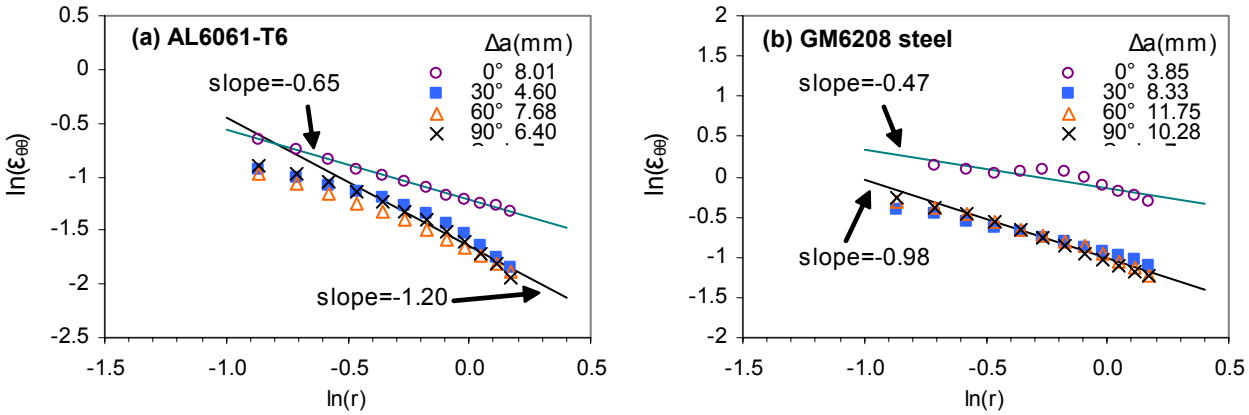

Fig.11: $\ln(\varepsilon_{\theta\theta})$ versus ln(r) near the crack tip with radial distance from crack tip r<1.2mm for (a) AL6061-T6 specimens, (b) GM6208 specimens in mixed mode I/III experiments.

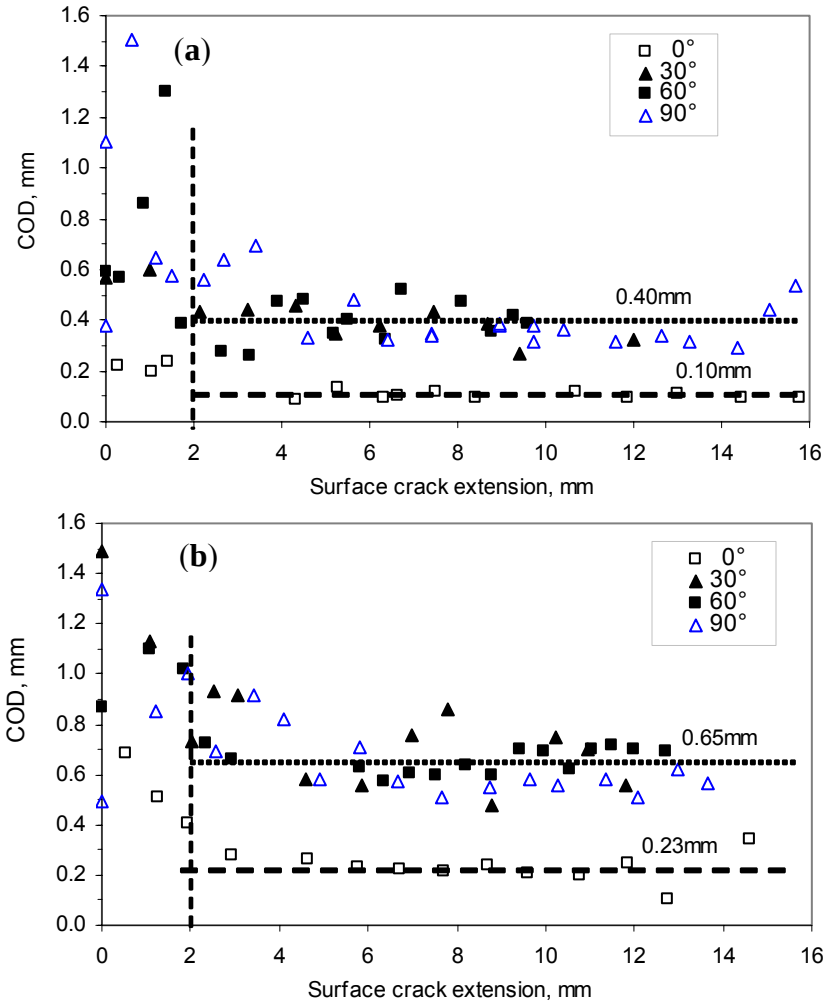

Fig.12: Total COD variations as a function of surface crack extension for (a) AL6061-T6 specimens, (b) GM6208 specimens loaded at Φ=0°, 30°, 60° and 90° in mixed mode I/III experiments.